Supplementary Information:

Rupali S. Mane[a], Sayli Pradhan[a], Vaishnavi Somkuwar[b], Rama Bhattacharyya[c], Prakash C Ghosh[d], Neetu Jha[a*]

[a]Department of Physics, Institute of Chemical Technology Mumbai, Nathalal Parekh Marg, Mumbai-400019 India.

[b]Center for Green Technology, Institute of Chemical Technology Mumbai, Nathalal Parekh Marg, Mumbai-400019 India.

[c]Centre for Research in Nano Technology and Science, Indian Institute of Technology Bombay, Mumbai-400076 India.

[d]Department of Energy Science and Engineering, Indian Institute of Technology Bombay, Mumbai-400076 India.

*Corresponding Author
Email: nr.jha@ictmumbai.edu.in

Abbreviations:

- d- interplanar distance
- a-lattice parameter
- *(hkl)*- miller indices
- D- crystal size
- k- lattice constant with value 0.9
- λ (nm)- wavelength of the X-ray source
- β - full width at half maxima (FWHM) in radians
- θ (degree)- is the angle of X-ray diffraction
- L_a- in plane distance

- C_λ -proportionality constant (4.4 nm)
- ECSA- electroactive surface area
- C_{dl}- double layer capacitance
- C_s- specific capacitance
- A- area of electrode (0.19625 cm^2)
- m- mass loading (0.151 mg)
- n- number of electrons
- F- faraday constant 96845 (C/mol)
- N_A- Avogadro number (6.03 $\times 10^{23}$ mol^{-1})
- Cp – specific capacitance (F/g)
- I - discharge current (A)
- Δt - discharge time (s)
- m - mass of the active material loaded on the electrode (mg/cm^2)
- E - energy density (Wh/Kg)
- P - power density (W/Kg)
- CR- capacity retention
- η - coulombic efficiency
- $C_{Dch(n)}$ - measured discharge capacity of cycle *n+1*
- $C_{Dch(n+1)}$ - measured discharge capacity of previous cycle *n*
- tD- time of discharge (s)
- tC- time of charge (s)

Formulas used:

Formulas:

1. d(Å) = $\frac{a}{\sqrt{h^2+k^2+l^2}}$ [1]

2. $D(mm) = \frac{K\lambda}{\beta COS\theta}$ 1

3. $La = \frac{4.4}{\sqrt{\frac{Ip}{Iq}}}$ 2

4. Distance of adjacent Co NPs 3

   $d_{Co} = 2(S(BET)/n\pi)^{1/2}$

5. $j_k = \frac{j \times jd}{(jd - j)}$ 4

   $j_d = 0.62nFD^{2/3}\omega^{1/2}v^{-1/6}\ Co_2$

6. $Cdi = Slope[\frac{\Delta J}{SR}]$ 5

   where $\Delta J = j_a - j_c$

7. $ECSA = \frac{Cdl}{Cs}$ 5

8. Specific Capacitance $= \frac{A}{scan\ rate \times m \times \Delta v}$ 6

9. Roughness factor (RF) $= \frac{ECSA}{Area\ of\ electrode}$ 7

10. Mass activity $= \frac{jK}{(mass\ loading)catalyst}$ 8

11. Active site g^{-1} (SDm) $= \frac{\int CV\ area \times N_A}{n \times scan\ rate \times F \times m}$ 6

12. $C_p = \frac{I \times \Delta t}{\Delta V \times m}$ 9

13. $E = \frac{1}{2}Cp(V)^2$ 10

14. $P = \frac{E*3600}{\Delta t}$ 10

15. $CR = \frac{C_{Dch(n+1)}}{C_{Dch(n)}} \times 100$ 11

16. $\eta = \frac{tD}{tC} \times 100$ 10

Table S1. Total yield of the catalyst

Name	Initial (W_I)	After pyrolysis (W_{F1})	After acid leaching (W_{F2})	Total yield (%) $(W_I – W_{FI})/W_I$ *100
ZIF 67	0.9301	-	-	-
AL-Co/NGC-600	0.9301	0.6854	0.543	41%
AL-Co/NGC-700	0.9301	0.6809	0.539	42%
AL-Co/NGC-800	0.9301	0.6712	0.526	43%
AL-Co/NGC-900	0.9301	0.6689	0.510	45.1%

Electrochemical measurements and electrode preparation:

The complete electrochemical experiment including CV, LSV, chronoamperometry test for stability, and methanol tolerance (MT) test were carried out at room temperature. A three-electrode set up connected to a potentiostat (PGSTAT 204) along with a rotor was used to carry out testing. The setup consists of a modified rotating disk electrode (RDE, 5 mm diameter and 0.19625 cm^2 area) as a working electrode, Ag/ AgCl electrode (with saturated 3 M KCl) was used as a reference electrode and platinum rod was used as a counter electrode. The measurement taken against Ag/AgCl, and converted to standard potential versus reversible hydrogen electrode (RHE) by using the following equation,

$$E_{RHE} = E_{Ag/AgCl} + 0.059*pH + E^0_{Ag/AgCl\ (0.199)}$$

Where, E_{RHE} –potential against RHE, $E_{Ag/AgCl}$ – potential against Ag/AgCl, and $E^0_{Ag/AgCl}$ standard electrode potential of Ag/AgCl. All the measurements were recorded after 20 cycles [12].

Electrode preparation for ORR study:

Originally, 3 mg of catalyst was dispersed in 1 ml of solvent which contains 960 µl of DMF and 40 µl of Nafion as a binder, the sample was then ultrasonicated for 30 min. Then electrode was polished before every measurement by using aluminium powder (1, 0.3, 0.05 mm)

followed by sonication for few minutes to remove all other content presents on the electrode surface and dried at room temperature. The working electrode was prepared by drop-casting 6 µl (0.151 mg / cm^2) of prepared ink on the working electrode followed by drying at room temperature. All the electrochemical measurements were carried out in both acidic (0.5 M H_2SO_4) and alkaline medium (0.1 M KOH). The obtained results were then compared with the commercial Pt/C (Pt on Vulcan XC-72, 20%) material with ink preparation same as above just instead of synthesized material Pt/ C was used.

Membrane electrode assembly (MEA) fabrication:

A 0.37 µm thick Teflon coated microporous carbon paper (AvCarb MGL 370) (MPL) was used as a starting material to prepare gas diffusion layer (GDL). The suspension for GDL was prepared as follow, Vulcan XC-72R powder along with 7 wt % Nafion solution and 40 wt % of platinum supported on Vulcan XC-72R carbon was added in isopropyl alcohol (IPA) and agitated in an PCi Analytics ultrasonic water bath for 30 minutes to make a uniform slurry. When the homogenous ink solution was ready it was evenly coated on the afore mentioned carbon backing layer by Prism ultracoat 300 (Ultrasonic Systems Inc.) instrument to get evenly distributed Pt loading on anode side (0.5 mg /cm^2). For the cathode side, same backing layer was used with modified ink. For ink preparation, AL-Co/NGC-800 catalyst powder was suspended in isopropyl alcohol (IPA) with 7wt % Nafion solution ultra-sonicated for 30 minutes. When the slurry was homogenous, it was brush-coated manually on the MPL and dried at 60 ºC for 5 minutes in each interval to get 15 mg /cm2 evenly distributed AL-Co/NGC-800 catalyst loading for cathode side.

MEA comprising membranes were obtained by sandwiching the membrane between the two electrodes. MEAs were evaluated using a Scribner fuel cell fixture (active area = 4 cm 2) with parallel serpentine flow field machined on graphite plates. The cell was tested at room temperature with humidified H2-O2 flow on each anode and cathode side. Measurements of

cell potentials with different current densities were recorded for drawing the polarization curve using electrochemical work station (BioLogic SP 150).

Fabrication of ZIHSC electrode:

The binder free electrode was fabricated by making catalyst ink, contains 10 mg of catalyst in 0.6 ml of DMF followed by 1 hr sonication. The resultant ink then drop casted on prior weighed carbon paper and dried at room temperature for 12 hr. The loading on carbon paper was maintained around 1.5 mg/cm^2. The electrochemical testing was done by two electrode sweglock cell assembly, where Zn foil was used as anode, filter paper was used as separator and 3 M $ZnSO_4$ was used as electrolyte. The entire study was done in range of 0.2 to 1.8 V of potential window.

Catalytic ORR measurements:

First, the electrolyte was purged with O_2 or N_2 for 30 min before the testing and measurement in a fresh electrolyte. All the potential was calibrated to the RHE (reversible hydrogen electrode). CV was performed with a potential window 0 to 1.2 V Vs RHE with a scan rate of 50 mV/ sec in series with N_2 and then O_2 saturated electrolyte. Before recording the final CV, the entire working electrode was stabilized by sweeping for 20 cycles former to each measurement. LSV was performed at 10 mV/sec within the 0 to 1.2 V Vs RHE in N_2 and O2 saturated (30 min) electrolyte with different rotation speeds (400, 625,900,1225, and1600 rpm). The entire polarization curve was obtained without current resistance (iR) compensation. The current densities were normalized by electrode area.

The K-L plot corresponding to the LSV curve at the different potential in diffusion limiting current was used to calculate electron pathway that is electron transfer number per oxygen molecule. The n value was calculated from the Koutechy-Levich equation. The linear fit between 1/ j (mA^{-1} / Cm^2) Vs $\omega^{-1/2}$ (rad/ sec)$^{-1/2}$ and slope value of this line were used to calculate n value. The K-L equation used is as follows:

$$\frac{1}{j} = \frac{1}{j_k} + \frac{1}{B * \omega^{1/2}}$$

Where j is measured current, j_k is diffusion limiting current, ω is rotation speed rate, B is reciprocal of the slope with the value calculated by using the equation:

$$B = 0.62nFC_{O2}{D_{O2}}^{2/3}\nu^{-1/6}$$

Where, n number electron transfer, F faradays constant (96485 C/ mol), C_{O2} the solubility of oxygen concentration in 0.1 M KOH (1.2×10^{-6} mol cm^{-3}), ${D_{O2}}^{2/3}$ is oxygen diffusion coefficient in 0.1 M KOH (1.90×10^{-5} cm^2S^{-1}) and ν is kinematic viscosity in 0.1 M KOH (0.01 cm^2S^{-1}).

Table S2 Obtained value of BET surface area and pore size distribution

Materials	**BET Surface Area (m^2/g)**	**Average Pore size (nm)**
ZIF 67	1402	1.6
AL-Co/NGC-600	290	1.26
AL-Co/NGC-700	410	1.28
AL-Co/NGC-800	470	1.49
AL-Co/NGC-900	530	1.29

Table S3 Structural study obtained from XRD and Raman

Name	**$d_{(hkl)}$ Å**	**D_{Co}**	**In plane distance (L_a)**
ZIF 67	5.26	-	-
AL-Co/NGC-600	2.04	6.7	4.78
AL-Co/NGC-700	2.38	8.07	4.63
AL-Co/NGC-800	2.54	8.65	4.44
AL-Co/NGC-900	2.62	9.1	4.19

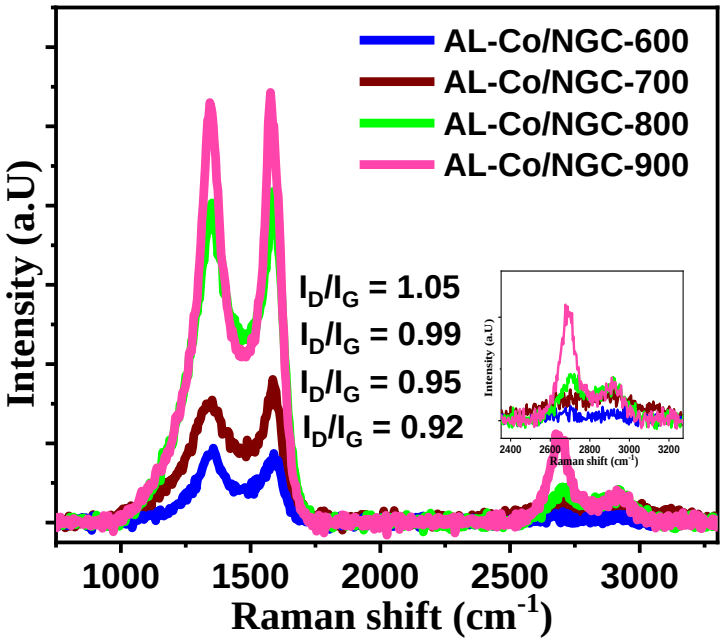

Fig. S1 Raman spectra of AL-Co/NGC-T (T= 600 to 900 ºC) catalysts, increase in I_D/I_G ratio reveal high degree of graphitization. Inset show 2D overtone peak of sample.

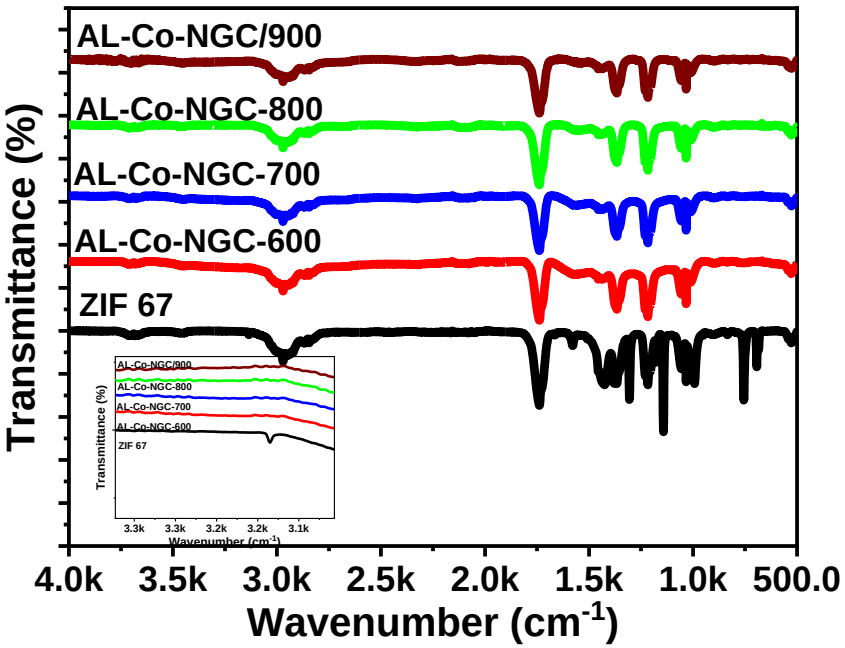

Fig. S2 FTIR study of as synthesized electrocatalyst

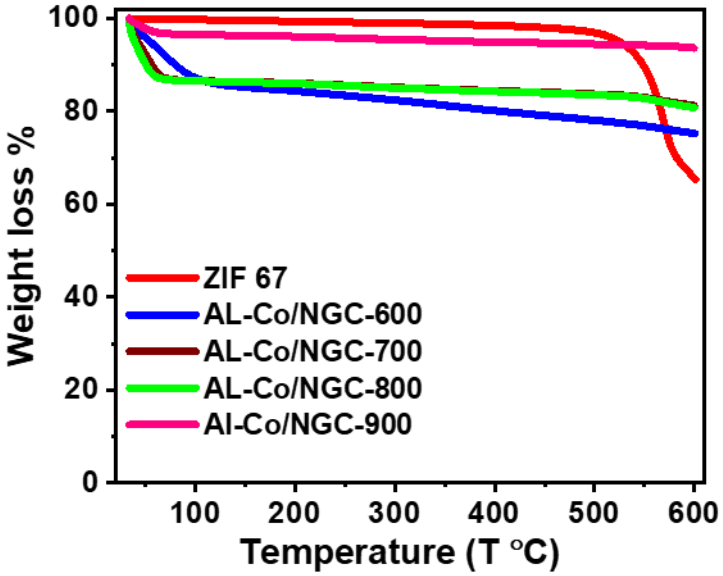

Fig. S3 Weight loss study obtained by TGA for ZIF 67 and acid treated pyrolyzed ZIF (AL-Co/NGC-T)

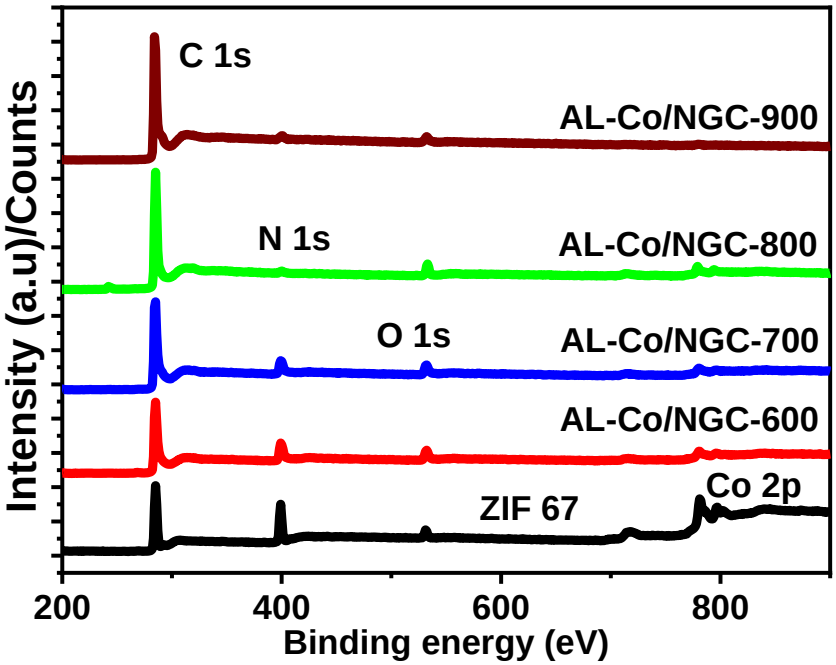

Fig. S4 XPS survey spectra of the catalysts

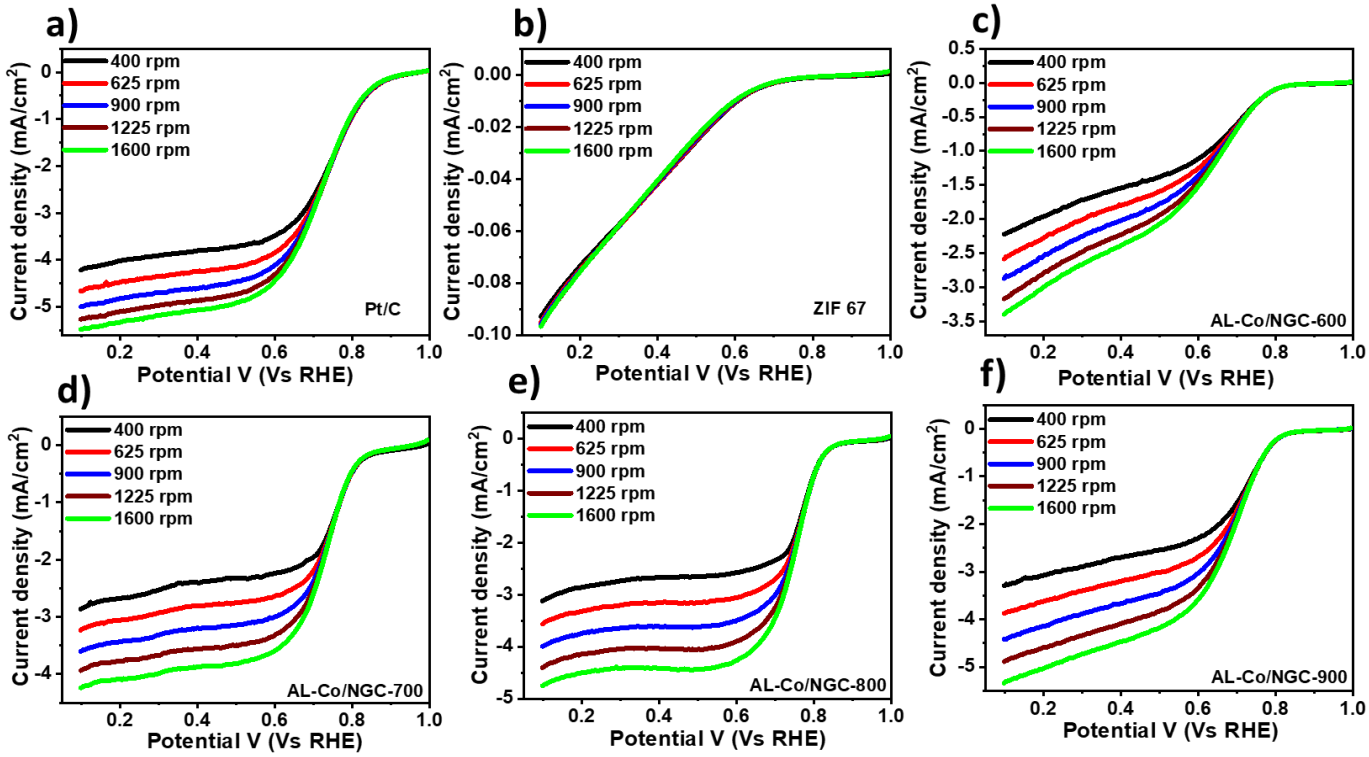

Fig. S5 LSV curve obtained at different rpm in acidic medium (0.5 M H_2SO_4) at 10 mV/sec for a) Pt/C, b)-f) AL-Co/NGC-600, AL-Co/NGC-700, AL-Co/NGC-800 and AL-Co/NGC-900

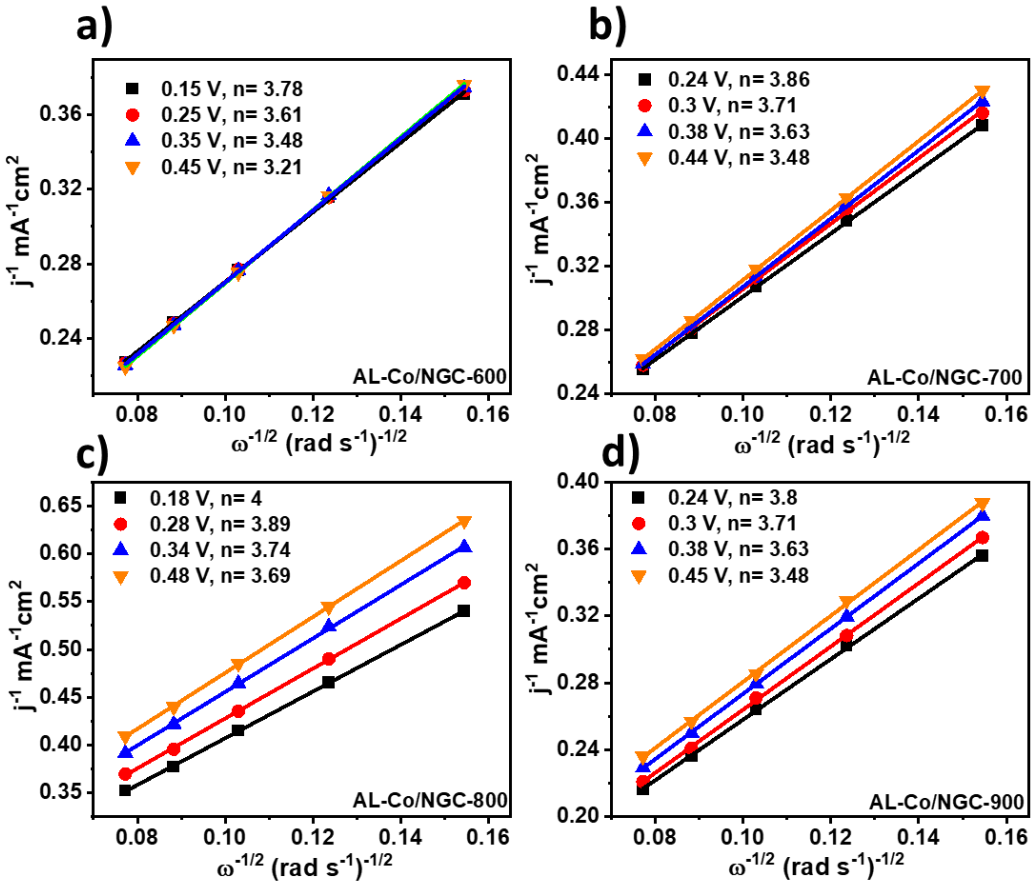

Fig.S6 K-L plot and electron transfer number (n) at different potential value in 0.5 M H_2SO_4 for AL-Co/NGC-T (T= 600 to 900 ºC).

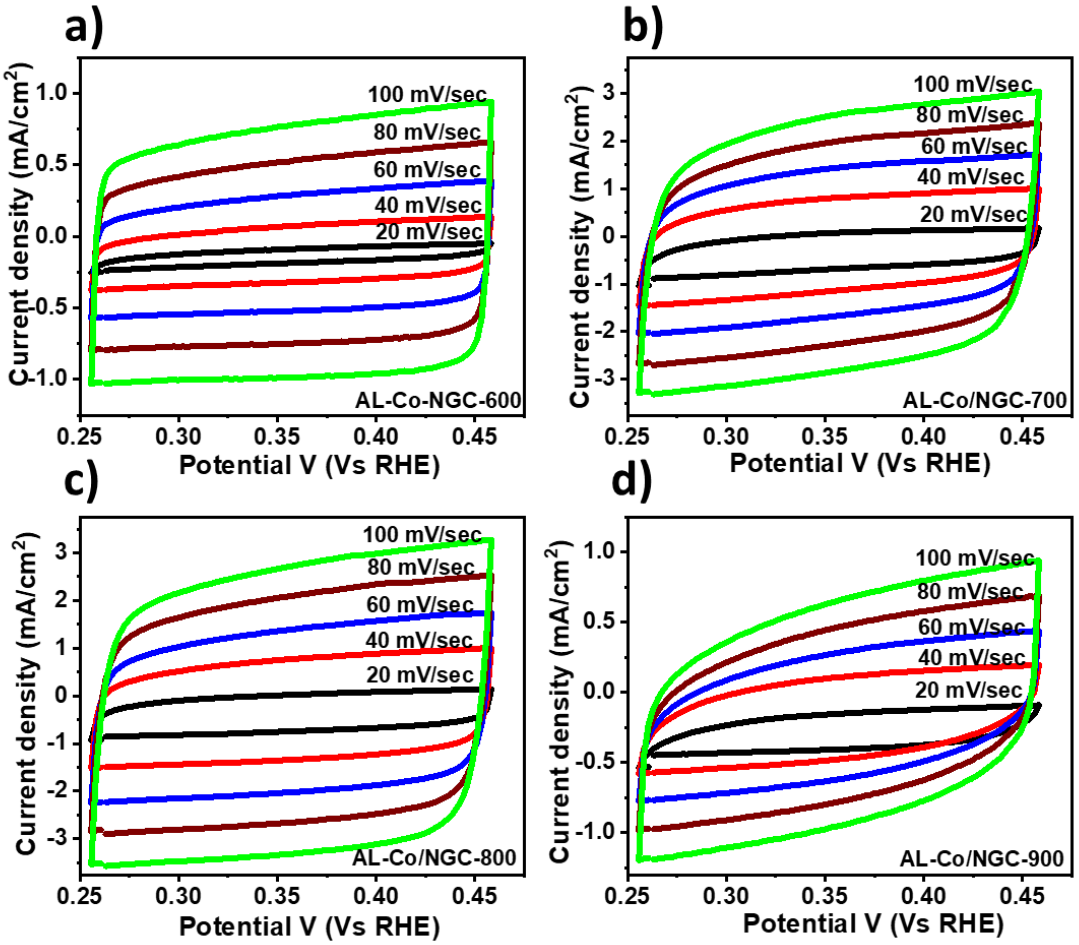

Fig. S7 CV obtained for AL-Co/NGC-T (T= 600 to 900 ºC) in non-faradic potential region in 0.5 M H_2SO_4 electrolyte at set of scan rate from 20 to 100 mV/sec with difference of 20 mV/sec.

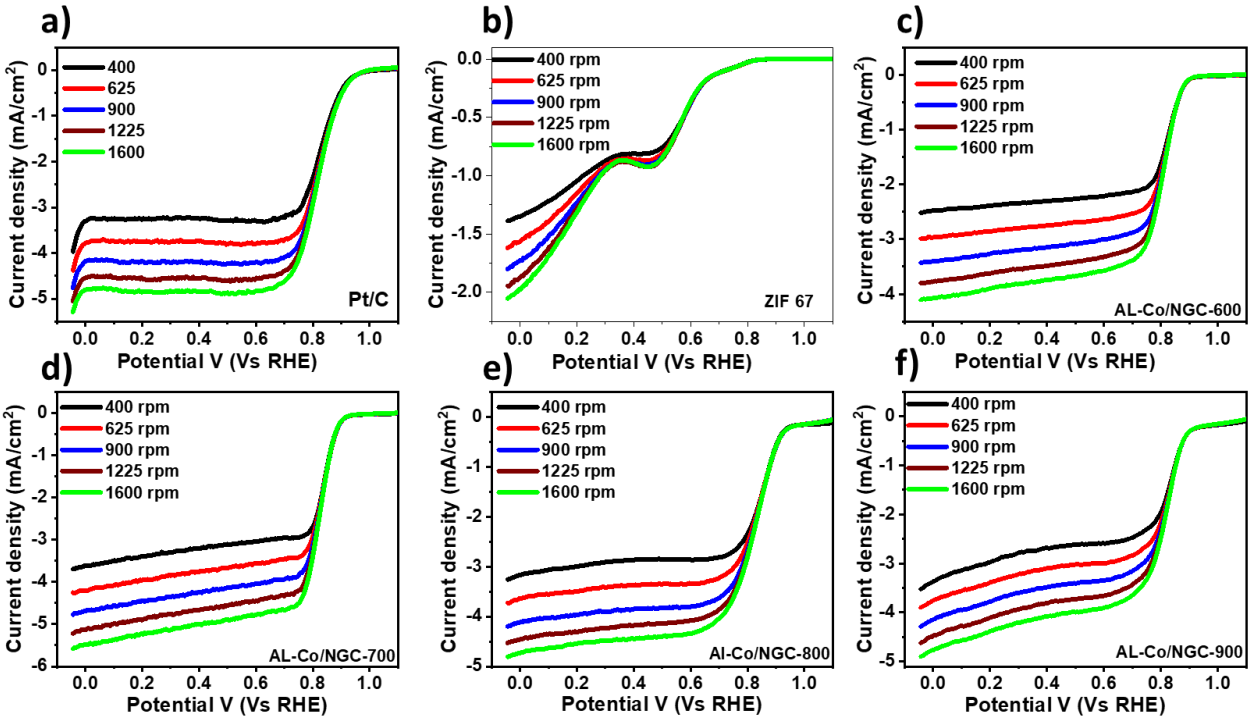

Fig. S8 LSV curve obtained at different rpm in alkaline medium (0.1 M KOH) at 10 mV/sec for a) Pt/C, b)-f) AL-Co/NGC-600, AL-Co/NGC-700, AL-Co/NGC-800 and AL-Co/NGC-900

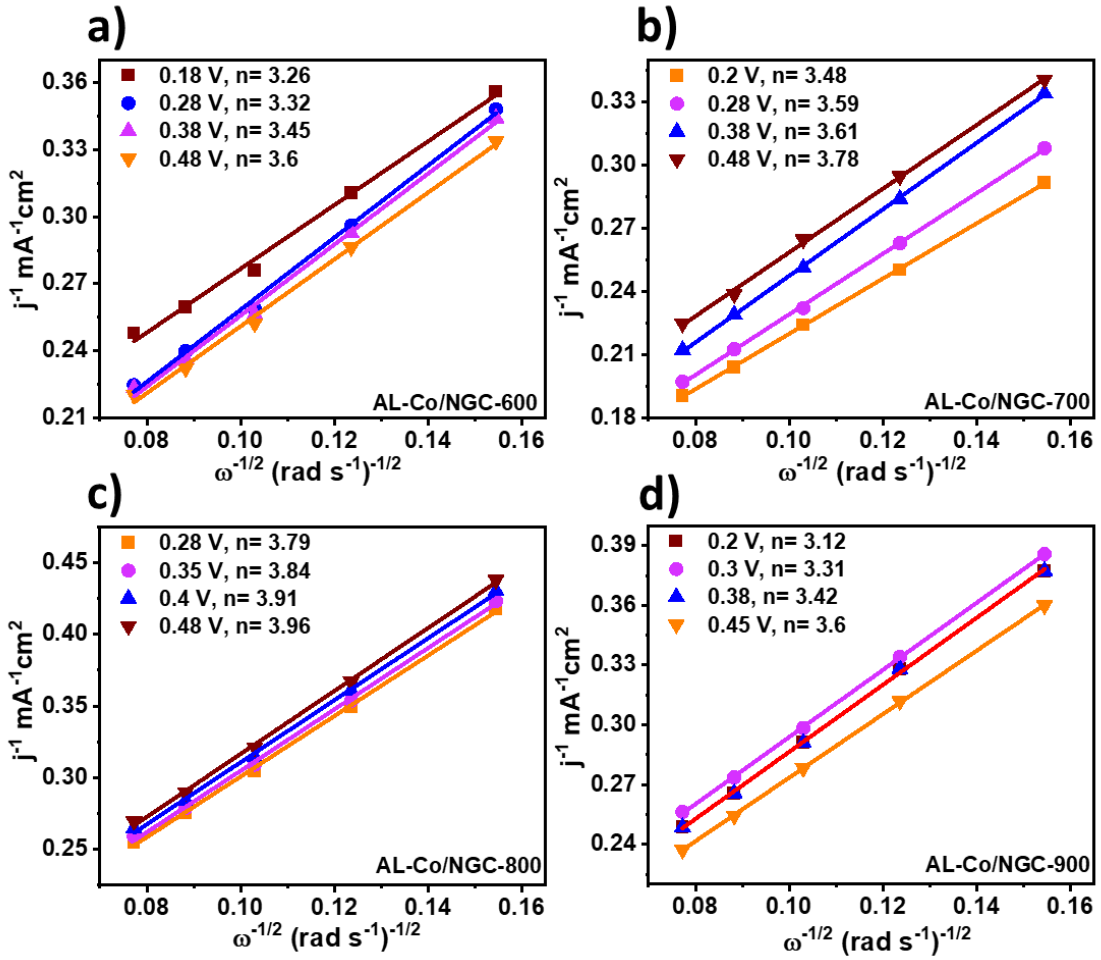

Fig.S9 K-L plot and electron transfer number (n) at different potential value in 0.1 M KOH for AL-Co/NGC-T (T= 600 to 900 ºC).

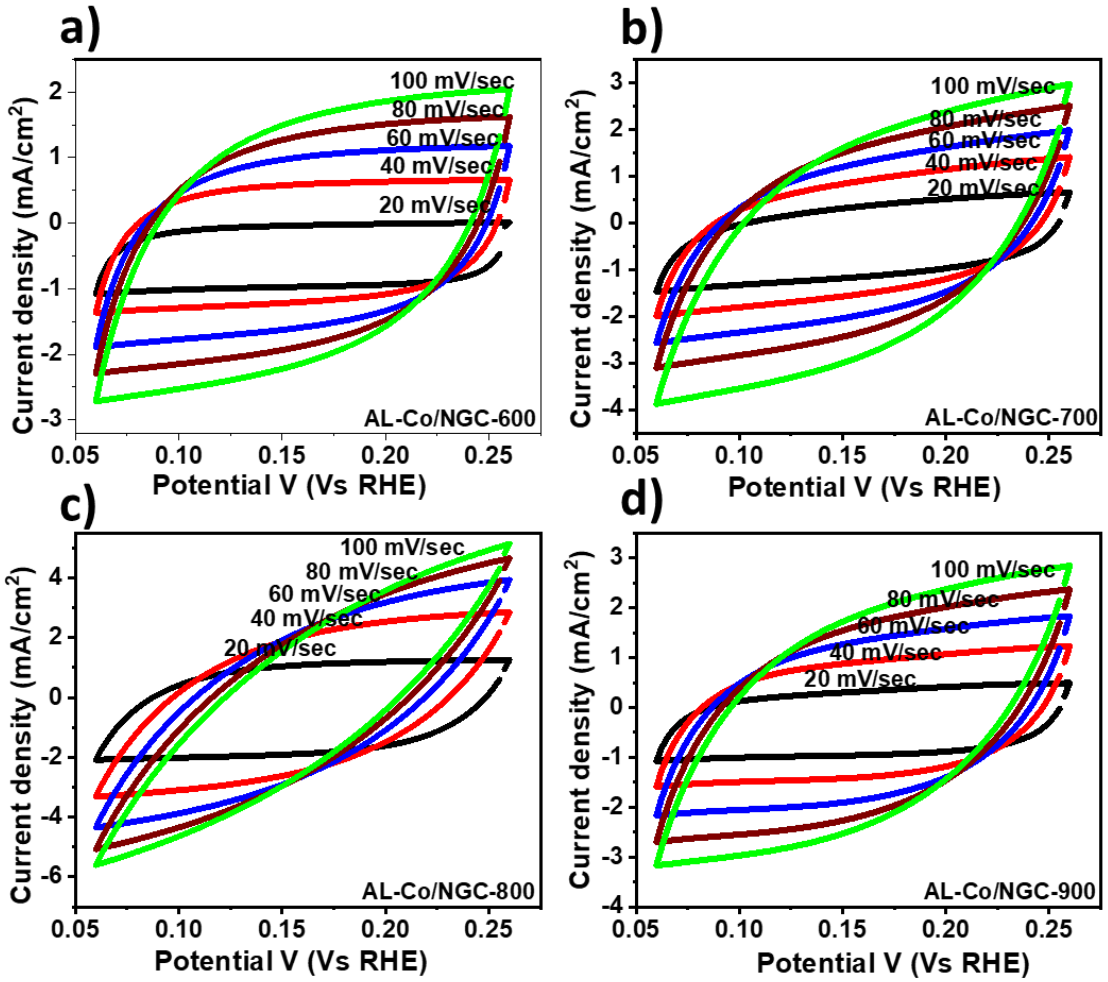

Fig. S10 CV obtained for AL-Co/NGC-T (T= 600 to 900 ºC) in non-faradic potential region in 0.1 M KOH electrolyte at set of scan rate from 20 to 100 mV/sec with difference of 20 mV/sec.

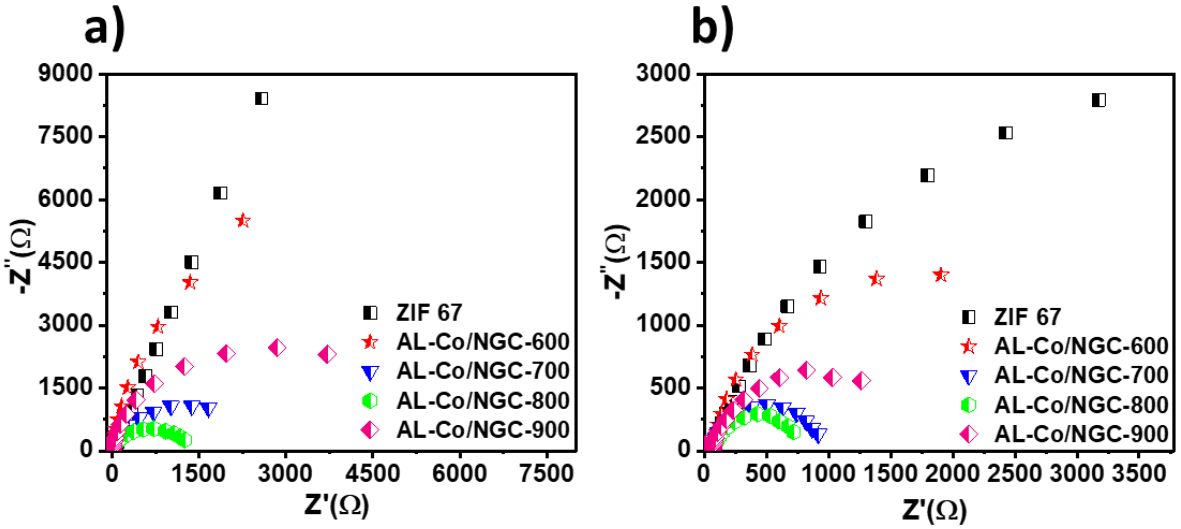

Fig.S11 Nyquist plot of as synthesized catalyst a) in 0.5 M H_2SO_4 b) 0.1 M KOH

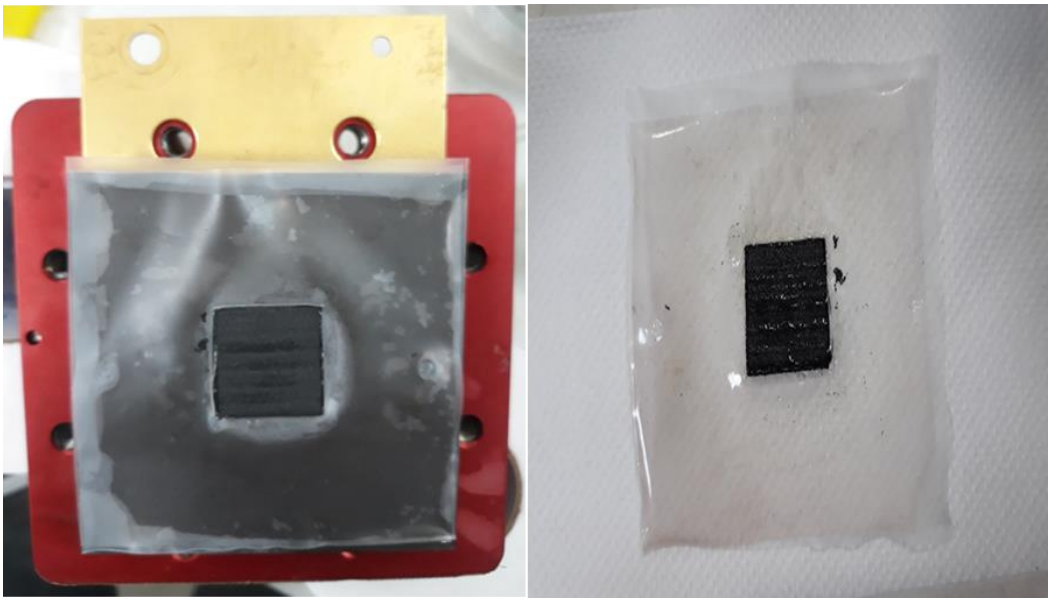

Fig.S12 a) Half-cell assembly of the fuel cell b) MEA after single cell testing

Table No. S4 Total contribution of active N species

Name	Co 2p	N1s At %					N_{metal}: N_{CN}	Work Function
	At % of Co	N_{pyri}	N_{pyro}	N_{gra}	N_{oxide}	Metal-N (Co-N)		
AL-Co/NGC-600	29.03	11.89	41.98	16.83	7.37	21.93	1.30	4.8
AL-Co/NGC-700	30.30	13.54	36.45	19.33	5.28	25.41	1.29	4.72
AL-Co/NGC-800	34.21	23.41	14.39	30.56	4.19	27.44	1.96	4.61
AL-Co/NGC-900	37.53	9.49	25.02	30.02	10.43	25.05	1.37	4.53

Table S5 comparative study obtained for pyrolyzed ZIF 67 with its effective parameters

Name	**Strategy/ concept**	**Synthesis procedure**	**Medium**	**Yield**	**BET Surface area**	**Application**	**Results**					
							Onset potential	**No. of electron (n)**	**Tafel**	**Double layer capacitance (C_{dl})**	**Active surface area (ECSA)**	**Ref**
ZIF-67-900	Co-Nx site	Pyrolysis (600-900 ºC), acid leaching (10 M HCL, hydrothermally)	Acid, Alkaline	-	501	ORR	0.93	~4 ~3.7	-	-	-	[4]
CoNC-900	Surface area, CoNx site	Pyrolysis (600-900 ºC)	50 mM PBS	-	237.8	ORR	-	3.92	-	-	-	[12]
Zn_xCo_{1-x}	Surface area	Pyrolysis (600ºC)	-	-	377	Potassium ion battery	-	-	-	-	-	[13]
CoNC3-1	ECSA, CoN_x	Pyrolysis (950ºC), acid leaching	Acid	41%	-	ORR	0.76	3.91	-	-	570	[5]
Co/Co-N_x-PCNSs	Co-Nx active site, graphitic shell	Triple pyrolysis 900 ºC	Alkaline	-	1155	ORR, OER, Zn air battery	0.98	3.9	59	-	-	[14]

Co@N-HCCs@NG	3D structure, surface area, work function	Evaporation-pyrolysis 900 ºC	Alkaline	-	618	ORR, OER	0.97	3.85		18.2	227	[15]
Co-MOF	High surface area, active sites	Solvothermal	Alkaline	-		ORR, OER	0.85	4	57	39		[16]
N, Co-CNSs-800	Active site	Pyrolysis (600-900 ºC)	Alkaline	-	-	ORR	0.96	3.99	59.7			[17]
Co-N-C	Effect of precursor	Pyrolysis, leaching	Acid, Alkaline	34%	1213	ORR, Zn air battery	0.89	4	68	82	-	[18]
C-N/Co (1/2)	Synthesis, Active site	Pyrolysis (920 ºC)	Alkaline	-	224.5	ORR, OER, Zn air battery	0.89	3.96	66	22.9	-	[19]
A-CoNC	High surface area, active sites	Pyrolysis, leaching	Alkaline	-	337.45	ORR, Zn air battery	0.91	3.84	55.8	13.28	-	[20]
ZIF-67-6	Synthesis strategy, Co-N_x site	Pyrolysis	Alkaline	-	388	ORR	0.91	3.59	-	-	-	[21]
CoFe@NC-SE	Surface area	Pyrolysis	Alkaline, acidic	-	659	ORR, Zinc air battery	0.93	3.8	62	22.5	562.5	[22]
$ACTP_5$@Co-N-800	Co-N_x site, Diffusion layer	pyrolysis	Alkaline	-	705	ORR, OER	1.0	4.03	74	31.44	786	[23]
Co/Co-N-C	Duel N doping strategy	Duel pyrolysis	Alkaline	-	701	ORR, Zinc air battery	0.99	~4	52.2	88.63	-	[24]

Co-HQ/C-800	Different N precursors	Pyrolysis	Alkaline	-	-	ORR	0.97	3.84	61	-	-	[25]
Co-N_x/Co@NMC	Synthesis strategy 2 D MOF, Co-N_x site	Pyrolysis	Acidic, Alkaline	-	319	ORR, Zinc air battery, OER	0.86	3.92	-	-	-	[26]
Co-Co_3O_4	Different N precursors	Hydrothermal, solvothermal, pyrolysis	Acidic, Alkaline	-	87.24	ORR, OER, HER	0.82	-	100.4	-	-	[27]
CoNC (1:4)	Mesopores, structure	Hydrothermal, polymerization, pyrolysis	Alkaline	-	310	ORR, Zinc air battery, OER	0.87	4.0	55	8.12	213	[28]
20Co-NC-1100	Synthesis strategy, Co-N_x site	Pyrolysis (600-1100 ºC)	Acidic, Alkaline	-	565	ORR	0.98	4	-	-	-	[29]
CoNC-900	Synthesis strategy, Co-N_x site	Pyrolysis	Alkaline	-	281	ORR	0.044 Vs Ag/AgCl	3.98	-	--	-	[30]
Purified Co_{15}-N-C-800	High temperature Co-N_x site	Pyrolysis (700-1000 ºC)	Alkaline	-	470	ORR	0.97	3.96	62	-	-	[31]
Co@C-800		Pyrolysis (600-2000 ºC)	Alkaline	-	369	ORR, OER	0.92	4	-	-	-	[32]
AL-Co/NGC-800	**Work function-based electron transfer, Co-N_x site**	**Pyrolysis (600-900 ºC)**	**Alkaline, acidic**	**45.1%**	**470**	**ORR, ZIHSC**	**0.951 0.85**	**3.91 3.89**	**69.4 82.5**	**22.65 33.44**	**647.14 811**	**This work**

Table S6 Overall review of obtained value for all parameters in this study

Name	Onset Potential (E_{onset}) V (Vs RHE)	Half-wave potential ($E_{1/2}$) V (Vs RHE)	Limiting current density (j_L) mA/cm^2	Number of electrons n	Tafel slop mV/dec	Double layer capacitance (C_{dl}) mF/cm^2	Active area (ECSA) cm^2	Roughness factor	Active site density (ASD) g^{-1}	Mass activity (mA/m $g_{catalyst}$)
Acidic										
ZIF 67	0.75	---	---	---	---	---	---		---	---
AL-Co/NGC-600	0.803	0.65	3.3	3.48	101.2	1.05	26.25	133.7	1.63×10^{23}	11.52
AL-Co/NGC-700	0.833	0.71	4.2	3.63	83	7.02	175.5	894.2	7.75×10^{23}	27.08
AL-Co/NGC-800	**0.85**	**0.72**	**4.8**	**3.89**	**82.8**	**32.44**	**811**	**4132.4**	**7.84×10^{23}**	**30.59**
AL-Co/NGC-900	0.828	0.75	5.3	3.71	96.3	27.34	683.5	3482.8	2.5×10^{23}	21.3
Alkaline										
ZIF 67	0.63	---	4.05	---	---	---	---	---		
AL-Co/NGC-600	0.883	0.812	4.56	3.45	83.7	16.01	457.42	2330.8	8.45×10^{23}	18.21
AL-Co/NGC-700	0.901	---	4.68	3.78	78	22.48	642.28	3272.7	1.09×10^{24}	16.55
AL-Co/NGC-800	**0.951**	**0.847**	**4.81**	**3.91**	**69.4**	**22.65**	**647.14**	**3297.5**	**1.51×10^{24}**	**21.32**
AL-Co/NGC-900	0.887	0.829	5.37	3.6	76	19.87	567.71	2892.8	1.02×10^{24}	18.67

Table S7 Literature study obtained for materials synthesized so far for ZIHSC study along with their effective parameters

Sr. No.	Materials	Precursors	Material Synthesis Method	Electrolyte	Specific Capacitance	Energy Density ($Whkg^{-1}$)	Power density (Wkg^{-1})	Cycling Stability	Potential window	Reference
1	Activated carbon	Coconut shell	Carbonization	1M Zn $(CF_3SO_3)_2$	170 Fg^{-1} at 0.1 Ag^{-1}	52 .7	1725	91%	0-1.8 V	[33]
2	Dense 3-D Graphene (DGH)	Graphene powder	Modified Hummers method	1M $ZnSO_4$	222.03 Fg^{-1} At 0.5 Ag^{-1}	118.42	600	80%	0.2-1.8V	[34]
3	Porous carbon Nano-sheets	Carbon	Salt template-assisted synthesis	3M $ZnCl_2$	78.6 $mAhg^{-1}$ at 0.5 Ag^{-1}	52.8	384.8	100%	0.2-1.6V	[35]
4	PPy/EGO composite	Pyrrole monomer, graphene oxide	One step electrochemical co-deposition method	1M $ZnCl_2$	444.2 Fg^{-1} at 0.35 Ag^{-1}	117.7	12400	81%	0.5 - 1.5V	[36]
5	OPCNF-20	PAN, zinc acetate dihydrate	Electrospinning	1M $ZnSO_4$	136.4 $mAhg^{-1}$ at 0.1 Ag^{-1}	97.74	9900	81%	0.2 -1.8 V	[37]
6	Activated carbon	Coconut shell	Steam activation method	3M Zn $(ClO_4)_2$	423.5 Fg^{-1}	190.3	89.8	80%	0-1.8V	[38]
7	MXene	Methanal, Melamine	Electrostatic self-assembly followed by pyrolysis	2M $ZnSO_4$	132 Fg^{-1} at 0.5 Ag^{-1}	54.9	3314.4	96.4%	0.2 - 1.8 V	[39]
8	HCN/SCN	Polyaniline-co-polypyrrole	Emulsion method	1M $ZnSO_4$	86.8 $mAhg^{-1}$ at 1.0 Ag^{-1}	59.7	447.8	98%	0.15–1.95 V	[40]

9	Nitrogen and sulphur co-doped carbon nanosheets (ACNS)	Thiourea, Citric acid	Evaporation	1M Zn $(CF_3SO_3)_2$	116.4 $mAhg^{-1}$ At 0.25 Ag^{-1}	95.9	206.3	102.7%	0-1.6V	[41]
10	BC-CNa	Bamboo powder, 2-methyl-imidazole	Combustion	2M $ZnSO_4$	51.4 $mAhg^{-1}$ at 0.2 Ag^{-1}	48.3	-	96%	0.2 -1.8V	[42]
11	PZC-A750	2-methylimidazole, PVP, PPy	Pyrolysis	1M Zn $(CF_3SO_3)_2$	124 $mAhg^{-1}$ at 0.25 Ag^{-1}	107.3	16647.7	65.9%	0-1.8V	[43]
12	N, O co-doped two-dimensional (2D) carbon nanosheet	Zinc nitrate hexahydrate, Urea	Annealing process	1 M $ZnSO_4$	111.0 $mAhg^{-1}$ at 0.1 Ag^{-1}	109.5	225	92.7%	0.2 - 1.8V	[44]
13	S-doped 3D porous carbon	Carbon source, pine needles	Pyrolysis	2M $ZnSO_4$	203.3 $mAhg^{-1}$ at 0.2Ag^{-1}	162.6	160	96.8%	0.2-1.8V	[45]
14	Activated Carbon	-	-	2M $ZnSO_4$	121 $mAhg^{-1}$ at 0.1Ag^{-1}	84	14900	91%	0.2-1.8V	[46]
15	Biowaste-derived porous carbon (PSC-A600)	Wood based pencil shavings	Pyrolysis	1M Zn $(CF_3SO_3)_2$	183.7 $mAhg^{-1}$ at 0.2Ag^{-1}	147	136.1	92.2%	0.2-1.8V	[47]
16	Porous Carbon nanosheets (PCNs)	Potassium nitrate, Starch powder	Pyrolysis	1M $ZnSO_4$	149 $mAhg^{-1}$ at 0.2Ag^{-1}	60	15976	91%	0.1–1.7 V	[48]
17	BN-CMTs	Polypyrrole , Boric acid	Annealing	1M $ZnSO_4$	416.6 $mAhg^{-1}$	472.6	1600	99.1%	0.2-1.8V	[49]

					at $1Ag^{-1}$					
18	O-doped porous carbon	Orange peels based activated carbon	Carbonization	1M $ZnSO_4$	125.7 $mAhg^{-1}$ at $1Ag^{-1}$	69.4	7570	92%	0.01-1.8V	[50]
19	N-doped porous carbon	Chitosan, $KHCO_3$, $Fe(NO)_3.9H_2O$	Simultaneous carbonization and activation	2M $ZnSO_4$	136.8 $mAhg^{-1}$ at $0.1Ag^{-1}$	191	3633.4	90.9%	0.2-1.8V	[51]
20	Hierarchical porous carbon	Bagasse, coconut shell	Hydrothermal carbonization	2M $ZnSO_4$+ 1M Na_2SO_4	305 $mAhg^{-1}$ at $0.1Ag^{-1}$	118	-	94.9%	0.01-1.8V	[52]
21	**AL-Co/NGC-800**	**ZIF67**	**Pyrolysis, acid leaching**	**3 M $ZnSO_4$**	**190 F g^{-1} 0.2 A g^{-1}**	**20.71 Wh kg^{-1}**	**3600 kWh kg^{-1}**	**97.04 %**	**0.2-1.8V**	**This work**

Reference:

1 P. Ch. Dey and R. Das, *Journal of Luminescence*, 2017, **183**, 368–376.

2 B. N. Sahoo and B. Kandasubramanian, *RSC Adv.*, 2014, **4**, 11331.

3 T. Chen, Y. Xu, S. Guo, D. Wei, L. Peng, X. Guo, N. Xue, Y. Zhu, Z. Chen, B. Zhao and W. Ding, *iScience*, 2019, **11**, 388–397.

4 X. Wang, J. Zhou, H. Fu, W. Li, X. Fan, G. Xin, J. Zheng and X. Li, *J. Mater. Chem. A*, 2014, **2**, 14064–14070.

5 A. Bharti and R. Natarajan, *ChemistrySelect*, 2021, **6**, 2298–2305.

6 M. F. Sanad, A. R. Puente Santiago, S. A. Tolba, M. A. Ahsan, O. Fernandez-Delgado, M. Shawky Adly, E. M. Hashem, M. Mahrous Abodouh, M. S. El-Shall, S. T. Sreenivasan, N. K. Allam and L. Echegoyen, *J. Am. Chem. Soc.*, 2021, **143**, 4064–4073.

7 M. A. Ahsan, T. He, K. Eid, A. M. Abdullah, M. L. Curry, A. Du, A. R. Puente Santiago, L. Echegoyen and J. C. Noveron, *J. Am. Chem. Soc.*, 2021, **143**, 1203–1215.

8 DST HySA Infrastructure Centre of Competence, Faculty of Engineering, North-West University, Potchefstroom, 2520, South Africa and I. Vincent, *Int. J. Electrochem. Sci.*, 2016, 8002–8015.

9 K. Mohanapriya and N. Jha, *Electrochimica Acta*, 2019, **324**, 134870.

10 D. J. Ahirrao, K. Mohanapriya and N. Jha, *Materials Research Bulletin*, 2018, **108**, 73–82.

11 A. Tornheim and D. C. O'Hanlon, *J. Electrochem. Soc.*, 2020, **167**, 110520.

12 S. You, X. Gong, W. Wang, D. Qi, X. Wang, X. Chen and N. Ren, *Adv. Energy Mater.*, 2016, **6**, 1501497.

13 Spontaneous Weaving of Graphitic Carbon Networks Synthesized by Pyrolysis of ZIF-67 Crystals - Zhang - 2017 - Angewandte Chemie International Edition - Wiley Online Library, https://onlinelibrary.wiley.com/doi/full/10.1002/anie.201701252, (accessed December 15, 2021).

14 W. Wu, L. Zong, X. Chen, W. Zhang, L. Cui, Y. Yang, X. Wang, S. Li and L. Wang, *Applied Surface Science*, 2021, **541**, 148262.

15 Y. Zhang, P. Wang, J. Yang, S. Lu, K. Li, G. Liu, Y. Duan and J. Qiu, *Carbon*, 2021, **177**, 344–356.

16 R. K. Tripathy, A. K. Samantara and J. N. Behera, *Dalton Trans.*, 2019, **48**, 10557–10564.

17 Y.-N. Hou, Z. Zhao, Z. Yu, Y. Tang, X. Wang and J. Qiu, *Chem. Commun.*, 2017, **53**, 7840–7843.

18 J. Gao, Y. Hu, Y. Wang, X. Lin, K. Hu, X. Lin, G. Xie, X. Liu, K. M. Reddy, Q. Yuan and H.-J. Qiu, *Small*, 2021, **17**, 2104684.

19 X. Liu, Y. Ma, Y. Cai, S. Hu, J. Chen, Z. Liu and Z. Wang, *RSC Advances*, 2021, **11**, 15722–15728.

20 L. Zhong, Q. Huang, J. Ding, Y. Guo, X. Wang, L. Chai, T.-T. Li, Y. Hu, J. Qian and S. Huang, *Journal of Power Sources*, 2021, **492**, 229632.

21 J.-P. Xuan, N.-B. Huang, J.-J. Zhang, W.-J. Dong, L. Yang and B. Wang, *Journal of Solid State Chemistry*, 2021, **294**, 121788.

22 A. Samanta and C. R. Raj, *Journal of Power Sources*, 2020, **455**, 227975.

23 J. Zhang, T. Zhang, J. Ma, Z. Wang, J. Liu and X. Gong, *Carbon*, 2021, **172**, 556–568.

24 D. Wang, P. Yang, H. Xu, J. Ma, L. Du, G. Zhang, R. Li, Z. Jiang, Y. Li, J. Zhang and M. An, *Journal of Power Sources*, 2021, **485**, 229339.

25 S. Chao, Q. Cui, Z. Bai, H. Yan, K. Wang and L. Yang, *International Journal of Hydrogen Energy*, 2014, **39**, 14768–14776.

26 H. Su, K.-X. Zhang, B. Zhang, H.-H. Wang, Q.-Y. Yu, X.-H. Li, M. Antonietti and J.-S. Chen, *J. Am. Chem. Soc.*, 2017, **139**, 811–818.

27 Q. Zhang, X. Zhao, X. Miao, W. Yang, C. Wang and Q. Pan, *International Journal of Hydrogen Energy*, 2020, **45**, 33028–33036.

28 L. Yang, N. Huang, C. Luo, H. Yu, P. Sun, X. Lv and X. Sun, *Chemical Engineering Journal*, 2021, **404**, 127112.

29 X. X. Wang, D. A. Cullen, Y. Pan, S. Hwang, M. Wang, Z. Feng, J. Wang, M. H. Engelhard, H. Zhang, Y. He, Y. Shao, D. Su, K. L. More, J. S. Spendelow and G. Wu, *Adv. Mater.*, 2018, **30**, 1706758.

30 S. Xie, S. Huang, W. Wei, X. Yang, Y. Liu, X. Lu and Y. Tong, *ChemElectroChem*, 2015, **2**, 1806–1812.

31 Y. Qian, Z. Liu, H. Zhang, P. Wu and C. Cai, *ACS Appl. Mater. Interfaces*, 2016, **8**, 32875–32886.

32 B. Chen, G. Ma, Y. Zhu and Y. Xia, *Sci Rep*, 2017, **7**, 5266.

33 H. Wang, M. Wang and Y. Tang, *Energy Storage Materials*, 2018, **13**, 1–7.

34 L. Zhang, D. Wu, G. Wang, Y. Xu, H. Li and X. Yan, *Chinese Chemical Letters*, 2021, **32**, 926–931.

35 H. Tian, R. Cheng, L. Zhang, Q. Fang, P. Ma, Y. Lv and F. Wei, *Materials Letters*, 2021, **301**, 130237.

36 J. Yang, J. Cao, Y. Peng, M. Bissett, I. A. Kinloch and R. A. W. Dryfe, *Journal of Power Sources*, 2021, **516**, 230663.

37 H. He, J. Lian, C. Chen, Q. Xiong and M. Zhang, *Chemical Engineering Journal*, 2021, **421**, 129786.

38 G. Yang, J. Huang, X. Wan, Y. Zhu, B. Liu, J. Wang, P. Hiralal, O. Fontaine, Y. Guo and H. Zhou, *Nano Energy*, 2021, **90**, 106500.

39 H. Cui, H. Mi, C. Ji, F. Guo, Y. Chen, D. Wu, J. Qiu and H. Xie, *J. Mater. Chem. A*, 2021, **9**, 23941–23954.

40 S. Chen, L. Ma, K. Zhang, M. Kamruzzaman, C. Zhi and J. A. Zapien, *J. Mater. Chem. A*, 2019, **7**, 7784–7790.

41 D. Wu, C. Ji, H. Mi, F. Guo, H. Cui, P. Qiu and N. Yang, *Nanoscale*, 2021, **13**, 15869–15881.

42 H. Chen, Y. Zheng, X. Zhu, W. Hong, Y. Tong, Y. Lu, G. Pei, Y. Pang, Z. Shen and C. Guan, *Materials Research Bulletin*, 2021, **139**, 111281.

43 X. Zhu, F. Guo, Q. Yang, H. Mi, C. Yang and J. Qiu, *Journal of Power Sources*, 2021, **506**, 230224.

44 G. Lou, G. Pei, Y. Wu, Y. Lu, Y. Wu, X. Zhu, Y. Pang, Z. Shen, Q. Wu, S. Fu and H. Chen, *Chemical Engineering Journal*, 2021, **413**, 127502.

45 D. Wang, S. Wang and Z. Lu, *Int J Energy Res*, 2021, **45**, 2498–2510.

46 L. Dong, X. Ma, Y. Li, L. Zhao, W. Liu, J. Cheng, C. Xu, B. Li, Q.-H. Yang and F. Kang, *Energy Storage Materials*, 2018, **13**, 96–102.

47 Z. Li, D. Chen, Y. An, C. Chen, L. Wu, Z. Chen, Y. Sun and X. Zhang, *Energy Storage Materials*, 2020, **28**, 307–314.

48 D. Wang, Z. Pan and Z. Lu, *Microporous and Mesoporous Materials*, 2020, **306**, 110445.

49 L. Han, H. Huang, J. Li, Z. Yang, X. Zhang, D. Zhang, X. Liu, M. Xu and L. Pan, *J. Mater. Chem. A*, 2019, **7**, 24400–24407.

50 J. Yu, L. Wang, J. Peng, X. Jia, L. Zhou, N. Yang and L. Li, *Ionics*, 2021, **27**, 4495–4505.

51 P. Liu, Y. Gao, Y. Tan, W. Liu, Y. Huang, J. Yan and K. Liu, *Nano Res.*, 2019, **12**, 2835–2841.

52 P. Yu, Y. Zeng, Y. Zeng, H. Dong, H. Hu, Y. Liu, M. Zheng, Y. Xiao, X. Lu and Y. Liang, *Electrochimica Acta*, 2019, **327**, 134999.